J Mater Sci (2010) 45:5012–5021
DOI 10.1007/s10853-010-4321-y

ICAM 2009

Magnetic field sensor based on a maghemite/polyaniline hybrid material

Fernando Gomes de Souza Jr. · Jéssica Alves Marins · José Carlos Pinto · Geiza Esperandio de Oliveira · Cezar Manzini Rodrigues · Luis Mauricio T. R. Lima

Received: 28 November 2009 / Accepted: 13 February 2010 / Published online: 6 March 2010

Abstract A hybrid material containing maghemite and polyaniline (PAni) doped with dodecylbenzenesulfonic acid (DBSA) was prepared through in situ polymerization in aqueous medium. The pure maghemite powder presented average particle diameter of 10 nm and magnetization force of 14 mN. The obtained maghemite/PAni hybrid material also presented nanometric dimensions, associated with reasonable electrical conductivity (260 times larger than the electrical conductivity of the pure maghemite) and about 60% of the original magnetic force. Additionally, the electrical conductivity of the hybrid powder showed significant sensitivity to changes of the magnetic field, indicating that these materials can be useful as magnetic field sensors.

F. G. de Souza Jr. (✉) · J. A. Marins
Instituto de Macromoléculas Professora Eloisa Mano, IMA/UFRJ, Universidade Federal do Rio de Janeiro, Cidade Universitária, CP 68525, Rio de Janeiro CEP 21945-970, Brazil
e-mail: fernando_gomes@ima.ufrj.br

J. C. Pinto
Programa de Engenharia Química/COPPE, Universidade Federal do Rio de Janeiro, Cidade Universitária, CP 68502, Rio de Janeiro 21945-970 RJ, Brazil

G. E. de Oliveira
Departamento de Química/CCE, Universidade Federal do Espírito Santo, Av. Fernando Ferrari, s/n, Goiabeiras, Vitória 29075-910, Brazil

C. M. Rodrigues
Instituto Federal do Espírito Santo (IFES), Unidade de Aracruz/ES, Av. Morobá S/N, Morobá, Aracruz E CEP 29199000, Brazil

L. M. T. R. Lima
Faculdade de Farmácia, Universidade Federal do Rio de Janeiro, Cidade Universitária, Rio de Janeiro 21945-970 RJ, Brazil

Introduction

Magnetic materials, such as ferrite and maghemite (γ-Fe_2O_3), have been extensively used for production of polymer composites intended for distinct applications [1–3]. The large surface area and unique magnetic properties of magnetic nanoparticles [4] allow the production of hybrid polymers that can be applied as imaging reagents [5], ferrofluids [6], toners [7], and magnetic sensors [8]. Among the many investigated magnetic nanoparticles, maghemite is known for their good chemical stability and large magnetization capability [4]. In addition, superparamagnetic maghemite does not retain the magnetization when it is not exposed to an external magnetic field [3]. This can be very important in some real applications, as particle aggregation induced by magnetic attraction, which can be avoided during processing of the material.

Polyaniline (PAni) is one of the most versatile and the cheapest conducting polymer material. PAni presents high electrical conductivity, easiness of preparation, stability to the heat and to the air, and low production costs. These characteristics can explain the successful use of PAni for the manufacture of different types of sensors [9, 10]. The main disadvantages of this conducting polymer, however, are its poor solubility in common organic solvents, the poor compatibility with common polymer materials, and the poor processability (due to the stiffness of its backbone), which makes the preparation of PAni composites very difficult sometimes [11]. For these reasons, the preparation of core–shell hybrid particles, containing an inorganic magnetic core coated by a conducting PAni shell, can constitute a complex task. Despite that the preparation of such hybrid particles can be extremely useful for many applications, including batteries, electrochemical display devices, molecular electronics, nonlinear optics, magnetic

sensors, electrical-magnetic shields, wave-absorbing materials, among others [12].

Aiming at the preparation of particles which can simultaneously present conducting and magnetic properties, maghemite/PAni hybrid materials were prepared through in situ polymerization in aqueous medium. The effect of the maghemite content on the electrical resistivity and magnetization force of the obtained hybrid materials was investigated with the help of probability distribution functions (which describe the spread of the electrical resistivity data). The materials were also characterized through Fourier transform infrared spectroscopy (FTIR), X-ray diffraction analysis (XRD), small angle X-ray scattering analysis (SAXS), and atomic force microscopy (AFM). Additionally, surface resistivity tests were performed on an interdigitated electrode, which was submitted to a magnetic field. In the best case, the electrical conductivity of the hybrid material under the magnetic field was about 30 times larger than the electrical conductivity of the pure PAni. The obtained results show that the prepared hybrids can be useful as magnetic sensing materials.

Experimental

Material

Ferric chloride ($FeCl_3$), sodium sulfite (Na_2SO_3), ammonium hydroxide (NH_4OH), aniline, and ammonium peroxydisulfate (APS) were supplied by Vetec (Rio de Janeiro, Brazil) as analytical grades. Dodecylbenzenesulfonic acid (DBSA) was supplied by Solquim LTDA (Rio de Janeiro, Brazil) as commercial grade. Reagents were used as received, without further purification.

Synthesis of maghemite

Maghemite was synthesized according to the usual preparation technique [13]. In a typical procedure, 30 mL of $FeCl_3$ solution (2 M), 20 mL of Na_2SO_3 solution (1 M), and concentrated NH_4OH were dissolved in 900 mL of water. After mixing of the reactants, a black powder precipitated. The supernatant was discarded and fresh water was added for washing of the precipitated powder. The procedure was repeated several times until reaching the pH of 7.0. The powder was filtrated and dried at room temperature. Finally, the dry powder was heated for 1 h at 200 °C in order to convert magnetite into maghemite.

Synthesis of polyaniline and hybrid materials

Polyaniline doped with dodecylbenzenesulfonic acid (PAni.DBSA) and the composites with maghemite (γ-Fe_2O_3) were synthesized through the one-step reaction route in aqueous medium. In a typical procedure, 4.7 mL (0.051 mol) of aniline and 16.7 g (0.051 mol) of DBSA were mixed in 250 mL of water/isopropanol (1:1 in volume) mixture under constant stirring [9, 11, 14]. The reaction mixture was kept at 0 °C, and an aqueous solution containing 11.36 g (0.051 mol) of APS in 40 mL of water was slowly added over a period of 20 min. After 6 h, the reaction mixture was poured into ethanol, filtrated, washed several times with ethanol, and dried. In the case of the maghemite/PAni composites (PAni.DBSA/γ-Fe_2O_3), the specified amount of γ-Fe_2O_3 was dispersed in the aqueous medium before addition of aniline and DBSA. After the polymerization, the PAni.DBSA/γ-Fe_2O_3 was precipitated in ethanol. The dark green precipitate was filtrated, washed several times with ethanol, and finally vacuum dried for 24 h.

Characterization

Attenuated total reflectance Fourier transform infrared (ATR-FTIR) spectroscopy

ATR-FTIR experiments were performed in a Bruker Spectrometer, model Alpha, using a diffuse reflectance accessory (ATR), at a spectral resolution of 4 cm^{-1} and with 128 accumulations. Samples were analyzed in the solid state over a trapezoidal Ge-crystal surface.

X-ray scattering

Wide and small X-ray scattering (WAXS/SAXS) measurements were performed at the beam line of the Brazilian Synchrotron Light Laboratory (LNLS, Brazil—D11A-SAXS1 #6597/07 and #7086/08) [15]. This beam line is equipped with an asymmetrically cut and bent silicon (111) monochromator ($\lambda = 1.743$ Å), which yields a horizontally focused X-ray beam. A linear position sensitive X-ray detector (PSD) and a multichannel analyzer were used to determine the SAXS intensity, $I(q)$, as function of the modulus of the scattering vector $q = (4\pi/\lambda)\sin\,\theta$, where 2θ is the scattering angle. All SAXS spectra were routinely normalized for the parasitic scattering intensity produced by the collimating slits, for the nonconstant sensitivity of the PSD, for the integrated beam intensity and sample thickness. As the incident beam cross-section at the detection plane is small, no mathematical deconvolution of the experimental SAXS function was needed [16].

Atomic force microscopy (AFM)

Atomic force microscopy was performed with the DI Nanoscope IIIa microscope of the LNLS, Campinas (LNLS, Brazil—AFM #8421/08), at noncontact mode, NSC-10-50, 20 N/m, and 260 kHz.

Surface resistivity

The electrical resistivity measurements of PAni.DBSA, γ-Fe_2O_3, and PAni.DBSA/γ-Fe_2O_3 were performed with the conventional four-point method, as reported elsewhere [8]. Materials were pressed into disk molds with 38 mm of diameter for 3 min, using a force of 4.5 ton. Average thickness was equal to 0.11 ± 0.02 cm. The experimental setup included a Keithley 6517A electrometer (acting as DC source and voltmeter) and a Minipa ET2907 multimeter (acting as amperimeter). Both devices were equipped with RS-232 interfaces for automatic data acquisition. Devices were coupled to a homemade four-probe device, with average probe distance of 0.17 ± 0.03 cm. The experimental data were recorded for 5 min, with sampling intervals of 1 s. [9, 17, 18].

Magnetic force

Magnetic force was determined with the help of an analytical balance and a digital caliper, described elsewhere [19]. Two removable supports were used for analyses: the first one was placed on the plate of the balance while the second one was placed outside the balance. The distance between the lower and higher tops was equal to 25.9 ± 0.2 mm. Tested materials were placed on the support located on the plate of the balance. The balance was unset, and a neodymium N42 magnet (external Gauss strength and energy density equal to 13.2 kg and 42 MGOe, respectively) was placed on the higher support. Variation of the mass was recorded, and magnetic force calculation (opposite to gravitational force) was calculated [19].

Magnetic sensitivity

An interdigitated electrode was used. The interdigitated area of the electrode was equal to $(1.7 \pm 0.3) \times 10^{-4}$ m^2. The analyzed materials were initially placed on the electrode surface. Soon afterward a 13.2-kg magnet was fixed under the electrode (thickness of 1 mm). Electrical resistivity was then evaluated in the absence and in the presence of the magnetic field. The electrical resistivity was also characterized with a Tenma 72-6900 multimeter. Data treatment was performed as presented previously [14]:

1. The initial resistivity (R_0) is assumed to be equal to the average resistivity value (R) obtained in the absence of the magnetic field.
2. The percentage variation of the sample conductivity ($\Delta\sigma$) is calculated in accordance with Eq. 1.

$$\Delta\sigma = \frac{100\left(R^{-1} - R_0^{-1}\right)}{R_0^{-1}} \quad (1)$$

Obtained $\Delta\sigma$ data depend on the composition of the analyzed material and on the presence of the magnetic field.

Probability density functions

Probability distribution functions are used to describe the spread of experimental data around a sample average. Probability distributions are generally represented in terms of integrals and can be interpreted as a smoothed histogram. The commonest PDF is the normal distribution, frequently used for computation of confidence limits of experimental data [20].

PDFs must satisfy the following requirements [20]:

1. PDFs are nonnegative everywhere;
2. The area bounded by PDFs is equal to 1 [21];
3. The probability for a random value to be within an interval is equal to the area bounded by the curve within this interval.

Most investigations assume that fluctuations of experimental data can be represented by a normal PDF. This approach is very useful for a large number of reasons, as described by Bard [22], and especially because of its simplicity. However, experimental fluctuations can follow rather different distribution functions, which can be used for interpretation of the experimental technique and of the experimental data. Particularly, electrical conductivity data and particle size distributions do not follow the normal distribution, which means that more involving analysis of available data must be performed for computation of confidence intervals [20]. Probability density functions were calculated here with numerical procedures written in Python, as reported elsewhere [11, 20].

Results

The amount of PAni in the PAni.DBSA/γ-Fe_2O_3 hybrid materials was obtained gravimetrically. The compositions of the prepared hybrid (maghemite/PAni) materials were equal to 8:92 (PAniMag8) and 25:75 (PAniMag25) in weight, with an estimated uncertainty of ±1%, respectively.

Figure 1 presents the ATR-FTIR of the pure materials and their hybrids. The ATR-FTIR spectrum of the pure PAni (see Fig. 1a) shows the characteristic bands described below. The wide band around 3330 cm^{-1} is related to stretching of OH. The small characteristic band next to 3000 cm^{-1} corresponds to C–H stretching and the doublet at 2922 and 2850 cm^{-1} is related to stretching of CH_2 and

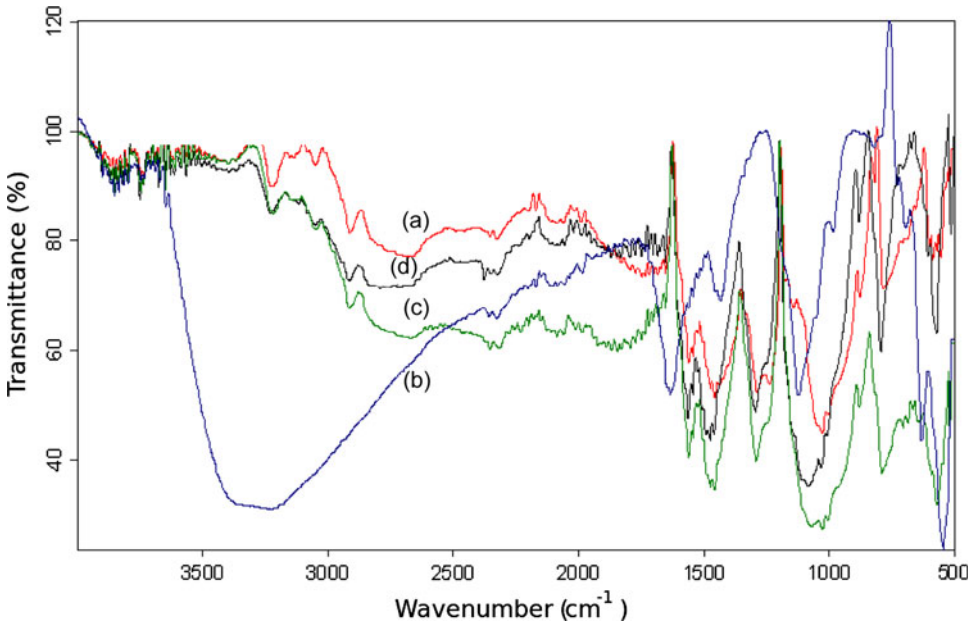

Fig. 1 ATR-FTIR spectra of PAni (*a*), maghemite (*b*), PAniMag8 (*c*), and PAniMag25 (*d*)

CH_3. The characteristic band at 1650 cm^{-1} is related to aliphatic C=C stretching. The doublet at 1455 cm^{-1} is characteristic of the C=C stretching of the aromatic ring. Bands at 1140 cm^{-1} correspond to stretching of the C–O bond of the phenol group. The characteristic stretching of the S=O bond appears around 1028 cm^{-1} and is conjugated with at least one characteristic band of the aromatic hydrogen, which also appears at 910 cm^{-1}. This explains the high intensity of this band. Other characteristic bands related to hydrogen are found at 875 and 597 cm^{-1} [23].

The ATR-FTIR spectrum of pure maghemite is also presented in Fig. 1b. The large characteristic band around 3420 cm^{-1} corresponds to the stretching of OH and is related to FeOH. The characteristic bands that appear at 1632 and 1433 cm^{-1} are related to presence of structural water. The band at 545 cm^{-1} is characteristic of Fe–O bound stretching [24, 25].

The ATR-FTIR spectra of the hybrids (see Fig. 1c, d) are very similar to the spectrum of PAni, even when the amount of maghemite is equal to 25% in weight. Besides, no significant displacement of the characteristic PAni bands can be observed in the hybrids, indicating that the chemical nature of the polymer is preserved during the in situ preparation of the composites.

Figure 2 presents the WAXS patterns of the maghemite, polyaniline, and hybrid materials. Polyaniline exhibits the six characteristics reflections at $2\theta = 15.0°$, 20.3°, 25.4°, 26.9°, 27.2°, and 35.5°. The presence of these peaks indicates that PAni possesses a pseudo-orthorhombic structure [17, 26–30]. These results agree with those of Fischer et al. [26], Lux [27] and Zilberman et al. [30] who observed reflections at similar angles for PAni powder prepared from solutions of concentrated sulfuric acid. The crystallinity degree of PAni is equal to (23 ± 2)% (see Table 1), which was calculated following the Ruland criterium [31]. This result is much smaller than the value of 80% reported previously by Gospodinova et al. [32]. Despite that PAni samples presented good electrical conductivity of $(1.4 \pm 0.2) \times 10^{-2}$ S/cm. This indicates that the obtained PAni presents semiconductor behavior useful for preparation of sensing materials, as demonstrated previously [11, 14, 17].

The WAXS pattern of the maghemite presented peaks at 18.3°, 30.2°, 35.6°, 43.3°, 53.3°, 57.3°, and 62.9°. According to Millan et al. [33], these peaks correspond to (111), (220), (311), (400), (422), (511), and (440) reflections of a spinel crystal structure such as that presented by maghemite or magnetite.

The composites present WAXS patterns that are similar to the ones of the pure materials. The increase of the maghemite content leads to the increase of the degree of crystallinity and raising of the characteristic diffraction peaks of the pure maghemite (see Fig. 5b, c). Therefore, the presence of maghemite causes the increase of the degree of crystallinity of the hybrid materials in comparison with pure PAni (see Table 1).

Crystal sizes were calculated with the Scherer's equation (Eq. 2) [34] and are also presented in Table 1.

$$CS = K \times \lambda / \Delta\theta \times \cos(\theta) \quad (2)$$

In Eq. 2, K is a constant (equal to 1.0), λ is the wavelength, θ is the Bragg angle ($2\theta/2$), and $\Delta\theta$ is the full width at half maximum (FWHM) of the (311) peaks. Pure maghemite presented crystal size of 11 ± 1 nm. The produced hybrids materials presented crystal sizes of 10 ± 1 and 12 ± 1 nm, indicating that the maghemite crystalline structure in the hybrids remained essentially the same. These values are

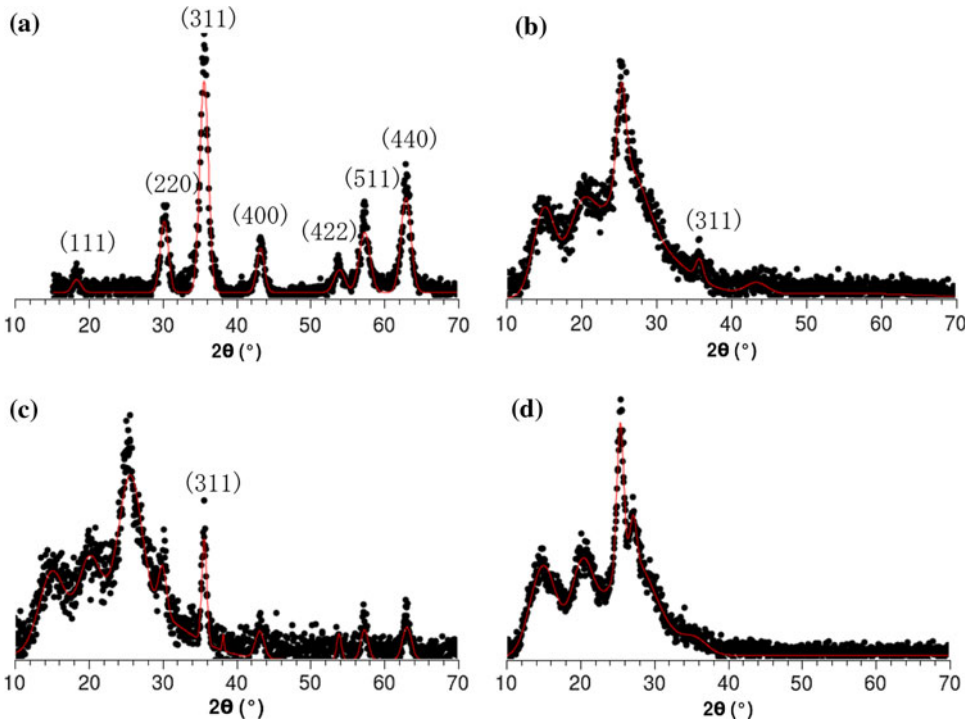

Fig. 2 WAXS diffractograms of pure maghemite (**a**), PAniMag8 (**b**), PAniMag25 (**c**), and PAni (**d**). *Dots* represent the experimental data while *lines* represent simulations performed using Fityk

Table 1 Crystallinity degree and confidence limits for particle diameter of the analyzed materials

Sample	Crystallinity (%)	CS (nm)[a]	Diameter (nm)
Maghemite	96 ± 1	11 ± 1	28^{+18}_{-14}
PAni.DBSA	23 ± 2	–	–
PAniMag8	28 ± 2	10 ± 1	43^{+12}_{-21}
PAniMag25	57 ± 2	12 ± 1	44^{+17}_{-27}

[a] CS calculated at (311) peaks using Scherrer equation (Eq. 2)

similar to the ones reported by Aphesteguy and Jacobo (~11 nm) [35] and Millan et al. (~9 nm) [33]. The obtained results indicate that the maghemite properties are probably preserved in the hybrids.

Characterization of the size distribution of maghemite particles is also very important because superparamagnetism can only be obtained in nanoparticles [36]. Figure 3 shows the AFM micrographs of the pure maghemite and hybrids materials. Figure 3a shows that maghemite particles present spherical morphology and nanometric size. Similar morphology can be observed in the hybrids, probably indicating that morphological properties of maghemite particles are also preserved in the hybrids.

Probability density functions were used to study the size distributions of the produced particles. Results are shown in Fig. 4 and in Table 1. Figure 4 shows that particle sizes follow asymmetric non-normal distributions. Given the monomodal character of the PDF, it seems plausible to say that particles do not agglomerate during preparation. However, the average sizes of maghemite particles in PAniMag8 and PAniMag25 are much larger than in the pure maghemite powder, indicating that maghemite particles were indeed encapsulated by polyaniline.

Scattering patterns for maghemite and hybrid materials are shown in Figs. 5 and 6, as observed experimentally and calculated with GNOM [37], respectively, based on available data. Table 2 also presents the radii of gyration (R_g) of the produced particles as calculated by GNOM, based on available data. The R_g of pure maghemite is equal to 9.6 ± 0.3 nm, while the R_g of the hybrids are equal to 25.5 ± 0.5 and 26.8 ± 0.1 nm, respectively. These values are in good agreement ($R^2 = 0.9999$) with results obtained from AFM, reinforcing that PAni probably covers the maghemite particles.

Calculations performed with the SAXS data also allowed the determination of the composition ($Comp_{SAXS}$) of the hybrid materials [37–40], as:

$$Comp_{SAXS} = \frac{100 \times P(r)_{max_{(h)}}}{P(r)_{max_{(mag)}}} \quad (3)$$

In Eq. 3, $P(r)_{max(h)}$ and $P(r)_{max(mag)}$ are the maxima of the distribution functions obtained for the hybrid and the maghemite presented in Fig. 6, respectively. As one can observe in Table 2, gravimetric and SAXS results are in very good agreement and present a correlation coefficient of 0.9969.

Figure 7 shows the magnetic force of maghemite and hybrid materials. Magnetic force data follow Gaussian distributions very closely. All tested materials presented

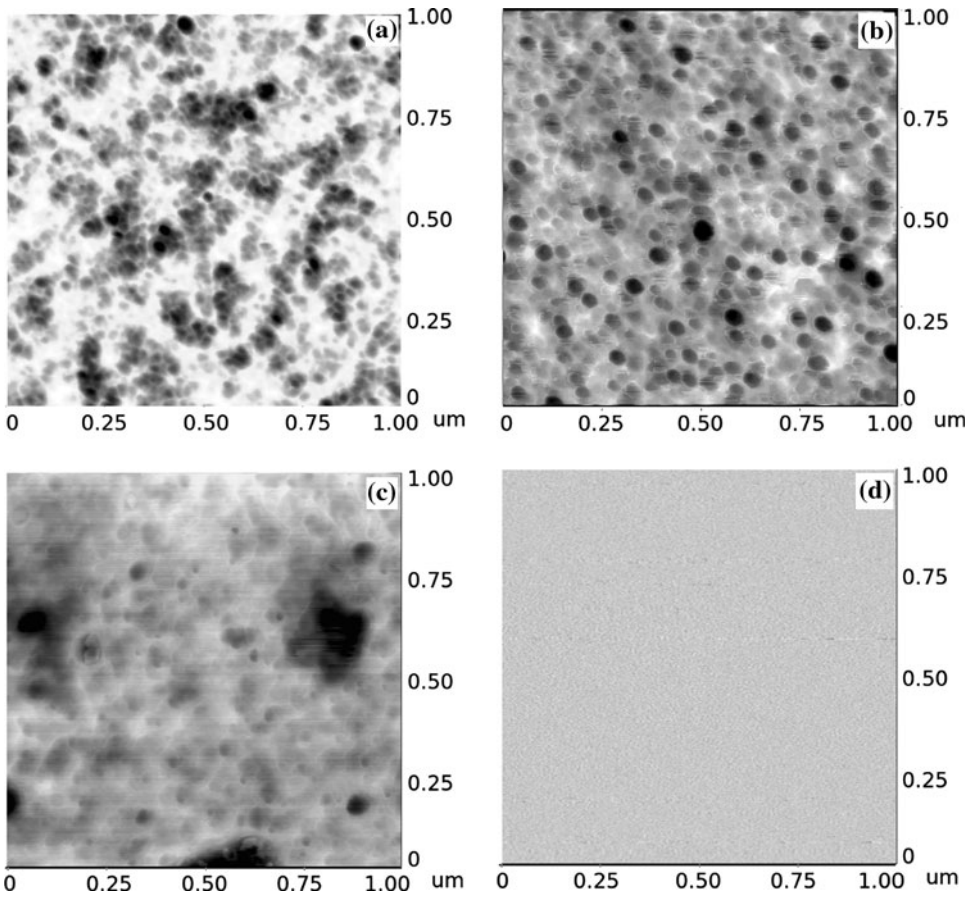

Fig. 3 AFM micrographs of maghemite (**a**), PAniMag8 (**b**), PAniMag25 (**c**), and pure PAni (**d**)

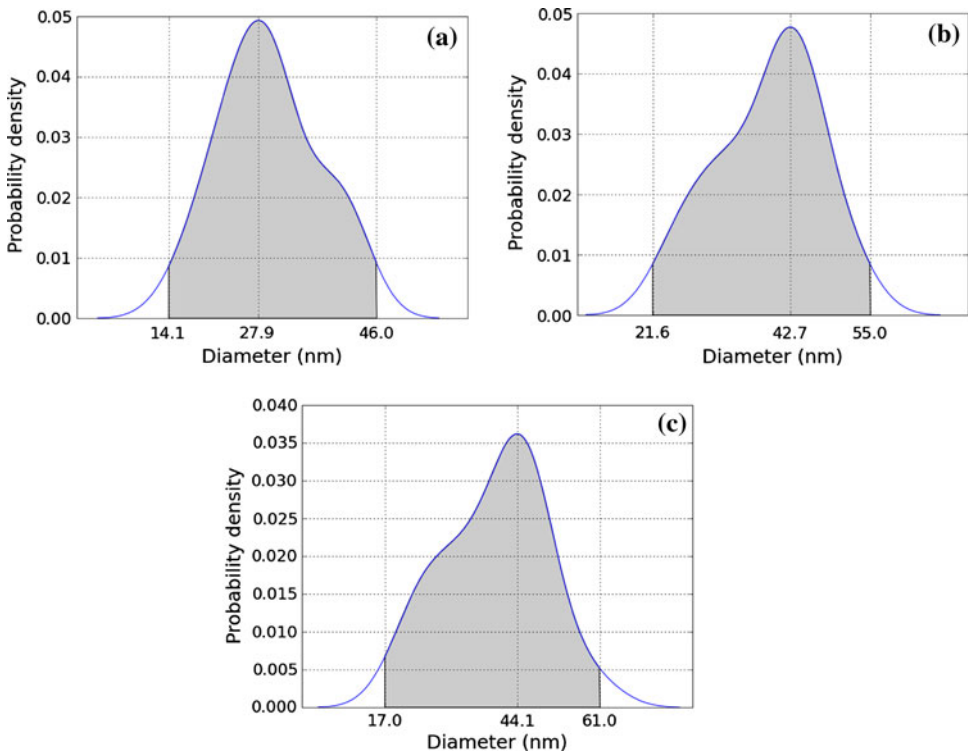

Fig. 4 PDF of size distributions of maghemite particles in pure maghemite (**a**), PAniMag8 (**b**), and PAniMag25 (**c**)

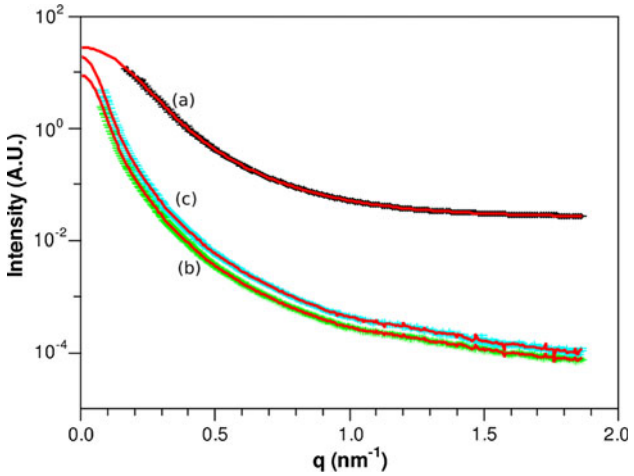

Fig. 5 SAXS diffractograms of pure maghemite (*a*), PAniMag8 (*b*), and PAniMag25 (*c*)

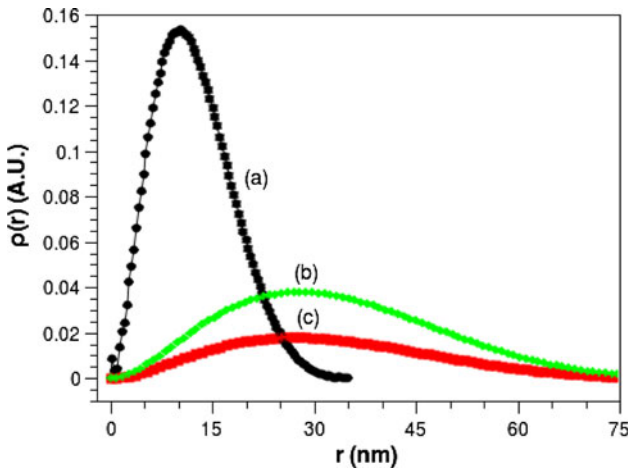

Fig. 6 Distance distribution functions obtained from SAXS data: pure maghemite (*a*), PAniMag8 (*b*), and PAniMag25 (*c*)

considerable magnetic force (with the exception of pure PAni, as one might already expect). The magnetic force of maghemite was equal to $14.31^{+0.55}_{-0.64}$ mN, while the magnetic forces of the hybrids PAniMag8 and PAniMag25 were equal to $6.00^{+0.14}_{-0.13}$ mN and $8.00^{+0.21}_{-0.14}$ mN, respectively. Thus, the hybrid material containing 8 wt% of maghemite retained 42% of the magnetic force, while the hybrid material containing 25 wt% of maghemite retained 56% of the magnetic force. These results indicate that the hybrid materials can be magnetized and used as pieces of magnetic devices.

Probability density functions of the surface resistivity of the produced materials are shown in Fig. 8. As shown in previous study [11], under DC field there is a strong autocorrelation of the electrical data along the experimental time, which makes clear that the experimental data may not be distributed at random. As a matter of fact, resistivity of polyaniline samples is subject to deterministic fluctuations, which can be ascribed to a number of reasons, including dynamic modification of the morphological characteristics of the analyzed material under the electrical DC field [11, 14, 19]. As one might already expect, pure maghemite presents the largest electrical resistivity, equal to $3.91^{+0.04}_{-0.02} \times 10^4\,\Omega\,\text{cm}$, while polyaniline presents the lowest electrical resistivity, equal to $7.14^{+0.25}_{-0.06} \times 10^1\,\Omega\,\text{cm}$. The hybrids PAniMag8 and PAniMag25 presented electrical resistivities of $1.52^{+0.04}_{-0.11} \times 10^2\,\Omega\,\text{cm}$ and $2.4^{+2.4}_{-0.8} \times 10^2\,\Omega\,\text{cm}$, respectively, which are 160 and 250 times lower than the resistivity of pure maghemite. Therefore, the modified materials simultaneously present good electrical and magnetic properties.

Surface resistivity was also evaluated under a magnetic field of 13.2 kg. The obtained results are shown in Fig. 9 and Table 3. Once again, obtained data do not follow a Gaussian distribution. Table 3 presents the surface resistivity of the tested materials with and without the presence of the magnetic field. Pure maghemite presents a small change of its surface resistivity in presence of the magnetic field, changing from $3.51^{+0.01}_{-0.02} \times 10^4$ (without magnetic field) to $3.37^{+0.02}_{-0.07} \times 10^4\,\Omega\,\text{cm}$ (in the presence of the magnetic field). This corresponds to a variation of $(4.22 \pm 0.02)\%$, which is possibly due to the better compaction of the material under the magnetic field. Differently, pure PAni presented the inverse behavior, characterized by a small rise of the surface resistivity. This behavior corresponds to a decrease of conductivity of $(-2.1 \pm 0.1)\%$; however, the observed change is not statistically significant, according to the calculated confidence interval. On the other hand, the hybrid materials presented a considerable change in surface resistivity under the magnetic field. The electrical resistivity of PAniMag8 changed from $3.6^{+0.4}_{-0.1} \times 10^2$ (without magnetic field) to $3.1^{+0.4}_{-0.1} \times 10^2\,\Omega\,\text{cm}$ (in the presence of the magnetic field), corresponding to a reduction of $(16 \pm 2)\%$, while the electrical conductivity of PAniMag25 changed from

Table 2 Radius of gyration and composition calculated by the SAXS model

Sample	Peak (nm)	R_g (nm)	$P(r)^a_{max}$	Comp_{SAXS} (%)	D_{max} (nm)
Maghemite	10.2	9.6 ± 0.3	$(1.53 \pm 0.01) \times 10^{-1}$	100.0 ± 0.5	35
PAniMag8	26.1	25.5 ± 0.5	$(1.80 \pm 0.01) \times 10^{-2}$	11.8 ± 0.1	75
PAniMag25	27.0	26.8 ± 0.1	$(3.79 \pm 0.02) \times 10^{-2}$	24.8 ± 0.2	75

[a] Maximum of the $P(r)$ function

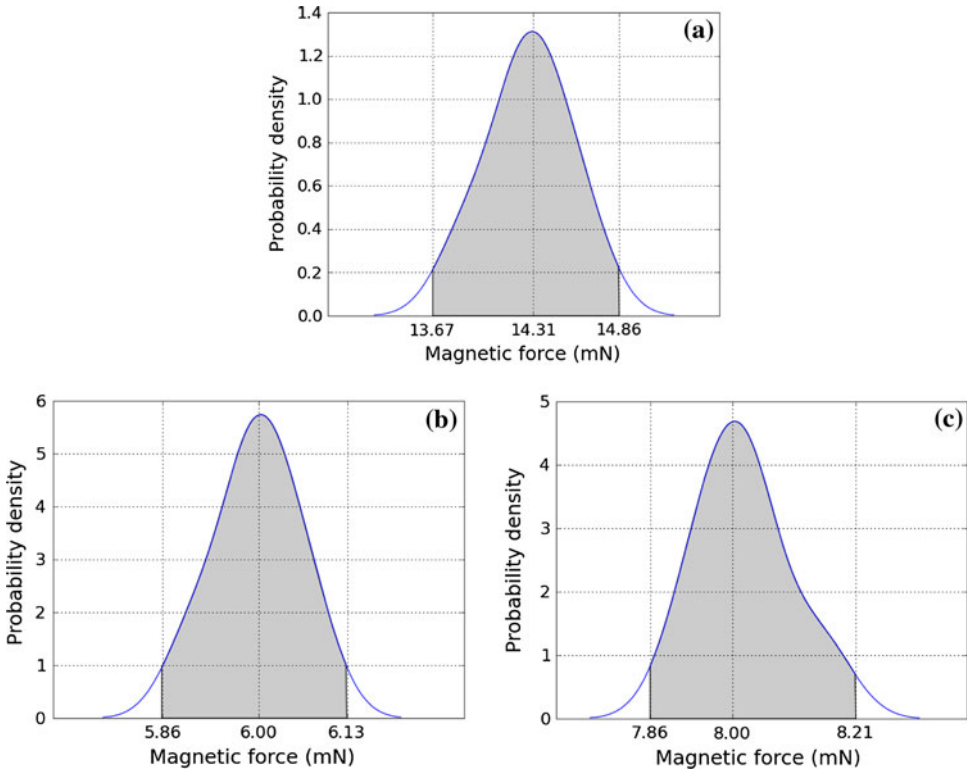

Fig. 7 Magnetic force modulus (mN) of pure maghemite (**a**), PAniMag8 (**b**), and PAniMag25 (**c**)

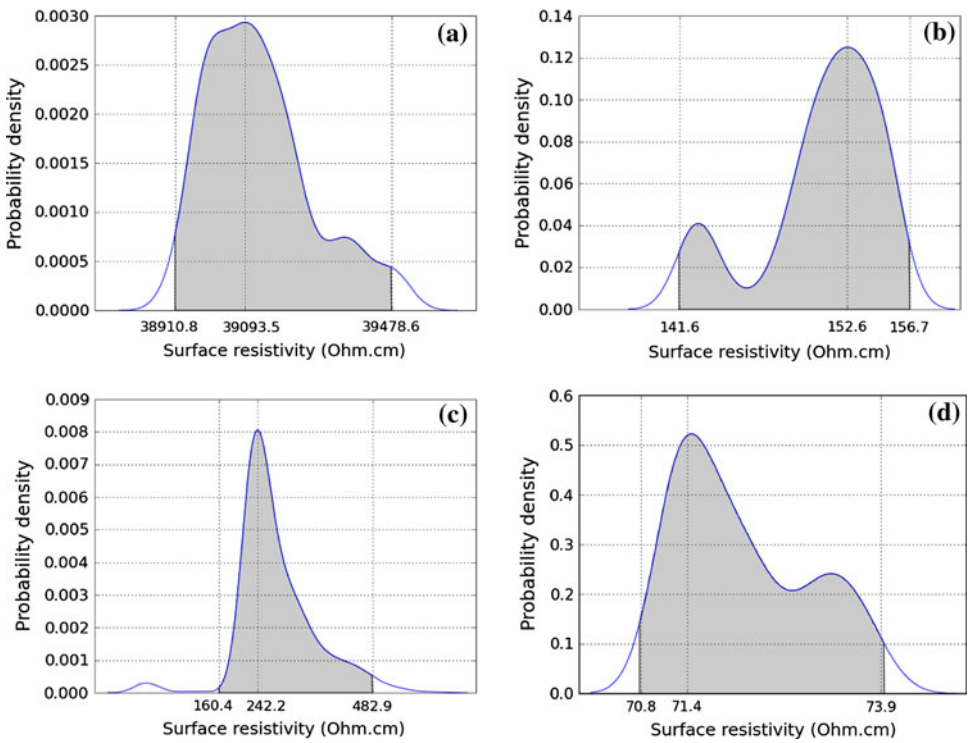

Fig. 8 PDFs of the surface resistivity: maghemite (**a**), PAniMag8 (**b**), PAniMag25 (**c**), and PAni (**d**)

$3.90^{+0.15}_{-0.05} \times 10^2$ (without magnetic field) to $2.35^{+0.14}_{-0.03} \times 10^2\ \Omega\,\mathrm{cm}$ (in the presence of the magnetic field), corresponding to a significant decrease equal to (66 ± 4)%. In the hybrid materials, maghemite particles are kept apart by PAni; under the magnetic field, the relative positions of the maghemite particles change, leading to significant increase of the contact points among PAni chains. This can probably explain why the surface resistivity changes with the magnetic field. As a consequence, maghemite/PAni hybrids constitute useful materials for magnetic field sensing applications.

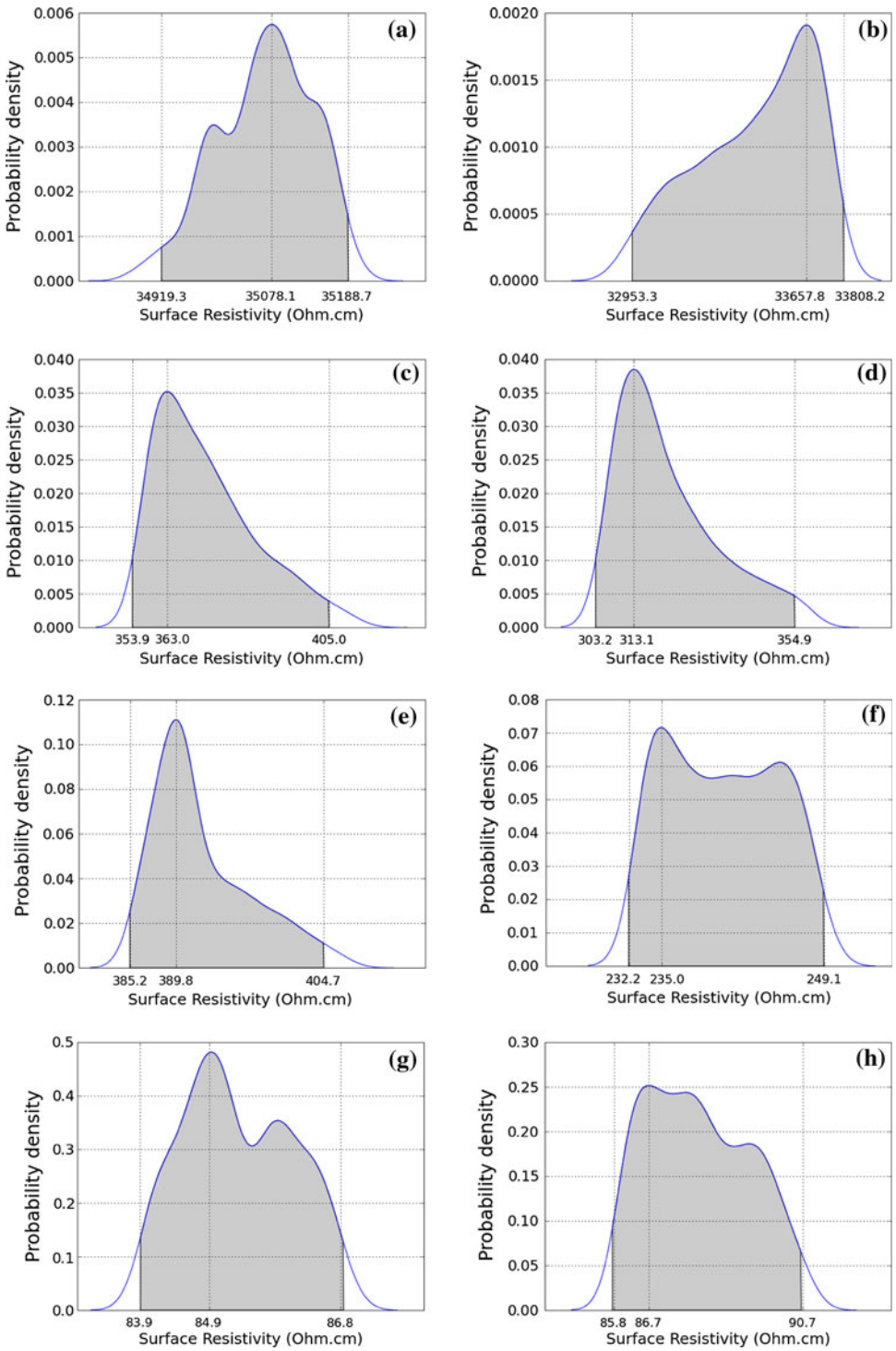

Fig. 9 PDFs of the surface resistivity before and after magnetic field application: pure maghemite (**a**)/(**b**), PAniMag8 (**c**)/(**d**), PAniMag25 (**e**)/(**f**), and PAni (**g**)/(**h**)

Conclusions

Hybrid maghemite/polyaniline (PAni) materials were prepared through in situ polymerization in aqueous medium and characterized. The obtained product presented a combination of good magnetic properties and relatively small electrical resistivity. ATR-FTIR results indicated that the chemical nature of the original materials was preserved in the hybrids. WAXS results showed that the crystalline characteristics of the materials were combined in the hybrids and that the presence of maghemite led to the rise of the degree of crystallinity of the composites. AFM analyses showed that the preparation technique produced particles with nanometric dimensions and prevented particle agglomeration.

As shown experimentally, the hybrid materials retained a considerable part of the original magnetic force of the

Table 3 Electrical resistivity and sensitivity to the magnetic field

Sample	Resistivity (Ω cm)		$\Delta\sigma$ (%)[a]
	At 0 G	At 13.2 kg	
Maghemite	$3.51^{+0.01}_{-0.02} \times 10^4$	$3.37^{+0.02}_{-0.07} \times 10^4$	4.22 ± 0.02
PAniMag8	$3.6^{+0.4}_{-0.1} \times 10^2$	$3.1^{+0.4}_{-0.1} \times 10^2$	16 ± 2
PAniMag25	$3.90^{+0.15}_{-0.05} \times 10^2$	$2.35^{+0.14}_{-0.03} \times 10^2$	66 ± 4
PAni	$8.5^{+0.2}_{-0.1} \times 10^1$	$8.7^{+0.4}_{-0.1} \times 10^1$	-2.1 ± 0.1

[a] Variation of the conductivity calculated according Eq. 1

maghemite particles, representing 56% of the magnetic force when the hybrid contained 25 wt% of maghemite. In addition, the hybrid materials presented much larger electrical conductivities (150–250 times larger), when compared to the electrical conductivity of pure maghemite. Besides, the electrical conductivity of hybrids containing 25 wt% of maghemite was sensitive to modification of the magnetic field (33 times larger in a field of 13.2 kg). Therefore, obtained results indicate that the produced maghemite/polyaniline hybrids may be useful as magnetic sensing materials.

Acknowledgements The authors thank CNPq—Conselho Nacional de Desenvolvimento Científico e Tecnológico (CNPq 577237/2008-0; CNPq 574358/2008-0; and CNPq 472009/2008-7); FAPERJ—Fundação Carlos Chagas Filho de Amparo à Pesquisa do Estado do Rio de Janeiro (FAPERJ E-26/112.116/2008)—and CAPES (Rede NanoBiotec) for the financial support and the scholarships. Authors also thank Brazilian Synchrotron Laboratory for the support on SAXS (D11A-SAXS1 #8507/09 and #9077/10) and AFM (#8421/08 and #9637/10) experiments.

References

1. Frisch HL et al (2001) J Phys Chem B 105:11901
2. Shouhu X et al (2009) Langmuir 25(19):11835
3. Kluchova K et al (2009) Biomaterials 30:2855
4. Boguslavsky Y, Margel S (2008) J Colloid Interf Sci 317:101
5. McHenry ME, Laughlin DE (2000) Acta Mater 48(1):223
6. Resensweig RE (1985) Ferrohydrodynamics. Cambridge University Press, Cambridge, p 344
7. McHenry ME, Majetich S, Artman JO, DeGraef M, Staley SW (1994) Phys Rev B 49(16):11358
8. Ripka P, Vertesy G (2000) J Magn Mater 215–216:795
9. Souza FG Jr, Anzai TK, Melo PA Jr, Nele M, Pinto JC, Soares BG (2008) J Appl Polym Sci 107:2404
10. Karyakin AA, Lukachova LV, Karyakina EE et al (1999) Anal Commun 36(4):153
11. Souza FG Jr, Soares BG, Pinto JC (2008) Eur Polym J 44:3908
12. Jianguo D, Xiaobing D, Wenchuan Z, Yuxing P, Jianhua W, Xingping L, Pei L, Albert SC (2002) Polymer 43(8):2179
13. Qu S, Yang H, Ren D, Kan S, Zou G, Li D, Li M (1999) J Colloid Interf Sci 215:190
14. Souza FG Jr, Michel RC, Soares BG (2005) Polym Testing 24:998
15. Kellermann G, Vicentin F, Tamura E, Rocha M, Tolentino H, Barbosa A, Craievich A, Torriani I (1997) J Appl Crystallogr 30:880
16. Souza FG Jr, Soares BG, Dahmouche K (2007) J Polym Sci Part B: Polym Phys 45:3069
17. Souza FG Jr, Sirelli L, Michel RC, Soares BG, Herbst MH (2006) J Appl Polym Sci 102:535
18. Souza FG Jr, Almeida M, Soares BG, Pinto JC (2007) Polym Testing 26:692
19. Davis RS (1993) Meas Sci Technol 4:141
20. Souza FG Jr, Pinto JC, Soares BG (2007) Eur Polym J 43(5):2007
21. O'Hagan A, Luce BR (2003) Bayesian initiative in health economics & outcomes research. Centre for Bayesian Statistics in Health Economics, p 57
22. Bard Y (1974) Nonlinear parameter estimation. Pergamon Press, New York
23. Silverstein RM, Bassler GC, Morril TC (2005) Spectrometric identification of organic compounds, 7th edn. John Wiley
24. Li L, Liu H, Wang Y, Jiang J, Xu F (2008) J Colloid Interf Sci 321:265
25. Boguslavsky Y, Margel S (2008) J Colloid Interf Sci 317:101
26. Fischer JE, Tan X, Scher EM, Cajipe VB, MacDiarmid AG (1991) Synth Met 41:661
27. Lux F (1994) Polymer 35:2915
28. Josefowicz ME, Epstein AJ, Pouget JP, Masters JG, Ray A, Sun Y, Tan X, MacDiarmid AG (1991) Synth Met 41:723
29. Pouget JP, Josefowicz ME, Epstein AJ, Tang X, MacDiarmid AG (1991) Macromolecules 24:779
30. Zilberman M, Titelman G, Siegmann A (1997) J Appl Polym Sci 66:243
31. Ruland W (1961) Acta Cryst 14:1180
32. Gospodinova N et al (2008) Macromol Rapid Commun 30(1):29
33. Millan A, Palacio F, Falqui A, Snoeck E, Serin V, Bhattacharjee A, Ksenofontov V, Gutlich P, Gilbert I (2007) Acta Mater 55:2201
34. Souza FG Jr, Richa P, Siervo A, Oliveira GE, Rodrigues CHM, Nele M, Pinto JC (2008) Macromol Mater Eng 293:675
35. Aphesteguy JC, Jacobo SE (2007) J Mater Sci 42:7062. doi: 10.1007/s10853-006-1423-7
36. Chen Q, Zhang ZJ (1998) Appl Phys Lett 73:3156
37. Svergun DI (1991) J Appl Cryst 24:485
38. Sonnberger R, Pfanner E, Dietz G (1986) Phys B Condens Matter 63:203
39. Bronstein LM, Kostylev M, Shtykova E, Vlahu T, Huang X, Stein BD, Bykov A, Remmes NB, Baxter DV, Svergun DI (2008) Langmuir 24:12618
40. Gelamo EL, Itri R, Tabak M (2004) J Biol Chem 279(32):33298